Computing high-order derivatives in compact integrated-RBF stencils

N. Mai-Duy[1,*], D. Strunin[2] and W. Karunasena[3]
[1] School of Mechanical and Electrical Engineering,
[2] School of Sciences,
[3] School of Civil Engineering and Surveying,
University of Southern Queensland, Toowoomba, QLD 4350, Australia

Submitted to *Engineering Analysis with Boundary Elements*, April 2021;
revised, September 2021

Abstract In Mai-Duy and Strunin (Eng Anal Bound Elem 125 (2021) 12-22) [1], it was shown that the inclusion of nodal values of high-order derivatives in compact local integrated-radial-basis-function (IRBF) stencils results in a significant improvement in the solution accuracy. The purpose of this work is to examine in detail the numerical performance of several approximation schemes based on one-dimensional IRBFs for computing high-order derivatives along the grid lines. The extended precision floating point arithmetic is utilised to achieve a high level of accuracy, and the efficiencies of the approximation schemes are improved by employing overlapping domain decomposition and mixed-precision calculations. In solving partial differential equations (PDEs), the proposed 1D-IRBFs are implemented using the RBF widths that are fixed and vary with grid refinement. A simple framework is presented to cover the two RBF width cases, and a numerical analysis is carried out for differential problems with slow and rapid variations in their solutions. In solving the convection-diffusion equations, the proposed 1D-IRBFs are also incorporated into the upwind schemes for effectively simulating highly-nonlinear flows. Numerical results show that high rates of convergence with respect to grid refinement are achieved with both fixed and variable

*Corresponding author E-mail: nam.mai-duy@usq.edu.au, Telephone +61-7-46312748, Fax +61-7-46312529

widths.

Keywords: high-order derivatives, high-order upwind schemes, compact approximations, integrated radial basis functions, two-dimensional 5-point stencils, RBF widths

1 Introduction

High-order methods, which are usually referred to as methods of at least third-order convergence, have gained increasing attention in recent decades. Examples of high-order methods include spectral methods [2], compact finite-difference (FD) methods [3] and RBF methods [4]. One can use spectral methods to solve a PDE defined on a simple domain to high accuracy if the solution to the problem is smooth. At lower accuracies, spectral methods still require less computer memory than the other methods. Compact FD methods have been used extensively as a substitute for spectral methods. However, it is not straightforward to extend compact FD schemes to irregular grids. On the other hand, RBF methods can be used to solve a PDE on a complex domain as they can work well with unstructured nodes. The RBF methods have been developed into three different types of discretisations: global (e.g. [4,5,6,7,8,9]), local (e.g. [10,11,12,13,14]) and compact local (e.g. [15,16,17,18]) schemes. The use of Cartesian grids to represent a complex domain in the RBF methods has received considerable attention in recent years owing to its efficient preprocessing (e.g. [16,19,20,21,22]).

An attractive feature of compact local FD/RBF schemes is that a high level of sparseness of the system matrix and a high level of accuracy of the solution can be achieved together. For one-dimensional compact 3-point and two-dimensional compact 5-point stencils, where nodal values of the second derivatives are included in the approximations, fourth-order convergence is typically obtained. In Mai-Duy and Strunin [1], it was shown that the inclusion of higher-order derivative values enables the order of grid convergence to be much higher than 4; however, the main focus of the work in [1] was the development of one-dimensional 3-point and two-dimensional 5-point stencils. Numerical calculation of high-order derivatives

presents a great challenge. Any error in the original function is magnified, and therefore results in much larger errors in its derivative functions. The main objectives of this work are to investigate several numerical schemes based on IRBFs in one dimension for computing derivatives along the grid lines, and how to utilise them in solving PDEs. Extended precision floating point arithmetic [23,24,25] is utilised. Large global systems are constructed and solved with standard/double precision (16-digit accuracy), while small local systems are handled using a higher level of numeric precision (32-digit accuracy). Utilisation of domain decomposition is explored to improve efficiency in solving local systems. In this work, two forms of the RBF widths, namely fixed and variable values with respect to grid refinement, are considered, and they are implemented in a simple framework. For the variable-width case, the RBF width is chosen as a linear function of the grid size. Utilisation of negative values of the slope is discussed for the first time. It should be pointed out that negative slopes can yield better accuracy for problems with rapid variations in their solutions. The proposed 1D-IRBF schemes are also utilised in the upwind schemes employed with the deferred-correction strategy [26] to maintain a high level of accuracy of the IRBF solution in simulating viscous flows.

The remaining of the paper is organised as follows. Section 2 is concerned with 1D-IRBF schemes for approximating a function and its derivatives, where extended precision and domain decomposition are explored to improve the quality of the IRBF approximations. The proposed 1D-IRBF schemes are incorporated into the two dimensional 5-point compact IRBF stencils for the solutions of Poisson's equation and the convection-diffusion equations in Section 3. Section 4 gives some concluding remarks.

2 Global one-dimensional IRBF schemes

For an IRBF scheme, one of the derivatives of function u is approximated using RBFs, and the approximate function u is then defined through integration. With $d^q u/dx^q$ taken as the derivative to be approximated by RBFs, the IRBF scheme can be mathematically described

as

$$\frac{d^q u(x)}{dx^q} = \sum_{i=1}^{N} w_i G_i(x) = \sum_{i=1}^{N} w_i I_i^{(q)}(x), \tag{1}$$

$$\frac{d^{q-1} u(x)}{dx^{q-1}} = \sum_{i=1}^{N} w_i I_i^{(q-1)}(x) + c_1, \tag{2}$$

$$\cdots \quad \cdots \quad \cdots$$

$$\frac{du(x)}{dx} = \sum_{i=1}^{N} w_i I_i^{(1)}(x) + c_1 \frac{x^{q-2}}{(q-2)!} + c_2 \frac{x^{q-3}}{(q-3)!} + \cdots + c_{q-1}, \tag{3}$$

$$u(x) = \sum_{i=1}^{N} w_i I_i^{(0)}(x) + c_1 \frac{x^{q-1}}{(q-1)!} + c_2 \frac{x^{q-2}}{(q-2)!} + \cdots + c_{q-1} x + c_q, \tag{4}$$

where N is the number of nodes on a grid line, $G_i(x)$ the RBF, $I_i^{(q-1)}(x) = \int I_i^{(q)}(x)dx$, $I_i^{(q-2)}(x) = \int I_i^{(q-1)}(x)dx$, $\cdots$, $I_i^{(0)}(x) = \int I_i^{(1)}(x)dx$, $(w_1, w_2, \cdots, w_N)$ the coefficients, and $(c_1, c_2, \cdots, c_q)$ the integration constants. In the of case of the multiquadric function, $G_i(x) = \sqrt{(x - x_i)^2 + a_i^2}$, where a_i is the width/shape-parameter and x_i the centre. The multiquadric function is a conditionally positive definite function; from a theoretical point of view, one needs to add to the interpolant a polynomial to acquire an invertible interpolation matrix. However, from numerical experiments reported, to our best knowledge, a singular interpolation matrix was never observed when the RBF approximations were not augmented with polynomial terms.

To replace the IRBF coefficients and integration constants in (1)-(4) with nodal values of u, equation (4) is applied at $x = x_i$, $i = (1, 2, \cdots, N)$, resulting in

$$\widehat{u} = \mathcal{C}\widehat{w}, \tag{5}$$

which is called the conversion system, $\mathcal{C}$ is the conversion matrix

$$\mathcal{C} = \begin{bmatrix} I_1^{(0)}(x_1), & I_2^{(0)}(x_1), & \cdots, & I_{N_x}^{(0)}(x_1), & \frac{x_1^{q-1}}{(q-1)!}, & \cdots, & x_1, & 1 \\ I_1^{(0)}(x_2), & I_2^{(0)}(x_2), & \cdots, & I_{N_x}^{(0)}(x_2), & \frac{x_2^{q-1}}{(q-1)!}, & \cdots, & x_2, & 1 \\ \cdots & & \cdots & & & \cdots & & \\ I_1^{(0)}(x_N), & I_2^{(0)}(x_N), & \cdots, & I_N^{(0)}(x_N), & \frac{x_N^{q-1}}{(q-1)!}, & \cdots, & x_N, & 1 \end{bmatrix},$$

and $\widehat{u}$ and $\widehat{w}$ are vectors

$$\widehat{u} = (u_1, u_2, \cdots, u_N)',$$

$$\widehat{w} = (w_1, w_2, \cdots, w_N, c_1, c_2, \cdots, c_q)'.$$

The minimum-norm solution to (5) is then substituted into (1)-(4).

Derivatives of u at $x = x_j$ can now be computed using nodal values of u

$$\frac{du_j}{dx} = \left[I_1^{(1)}(x_j), \cdots, I_N^{(1)}(x_j), \frac{x^{q-2}}{(q-2)!}, \cdots, 1, 0 \right] \mathcal{C}^{-1}\widehat{u}, \quad j = (1, 2, \cdots, N) \tag{6}$$

$$\cdots \quad \cdots \quad \cdots \quad \cdots \quad \cdots \quad \cdots$$

$$\frac{d^q u_j}{dx^q} = \left[I_1^{(q)}(x_j), \cdots, I_N^{(q)}(x_j), 0, \cdots, 0, 0 \right] \mathcal{C}^{-1}\widehat{u}, \quad j = (1, 2, \cdots, N) \tag{7}$$

or

$$\widehat{\frac{du}{dx}} = \mathcal{D}_1 \widehat{u}, \tag{8}$$

$$\cdots \quad \cdots \quad \cdots$$

$$\widehat{\frac{d^q u}{dx^q}} = \mathcal{D}_q \widehat{u}, \tag{9}$$

where

$$\widehat{\frac{d^k u}{dx^k}} = \left(\frac{d^k u_1}{dx^k}, \frac{d^k u_2}{dx^k}, \cdots, \frac{d^k u_N}{dx^k} \right)', \quad k = (1, 2, \cdots, q),$$

and $\mathcal{D}_k$ is the differentiation matrix for computing nodal values of the kth-order derivative of u.

The IRBF scheme is said to be of order q (denoted by IRBFq) if RBFs are used to approximate the qth-order derivatives. For IRBFq, the RBFs and their integrated basis functions can be used to compute derivatives of orders up to q. To compute derivatives of higher orders, derivative functions can be taken as the original function. In this work, three IRBF schemes, namely IRBF2, IRBF4 and IRBF6, are considered, and we are interested in computing the

derivatives of orders up to 6. For each scheme, we take the differentiation matrices $\mathcal{D}_1$ and $\mathcal{D}_2$ as the base, and compute the derivatives of u according to

$$\widehat{\frac{du}{dx}} = \mathcal{D}_1^{(q)}\widehat{u}, \tag{10}$$

$$\widehat{\frac{d^2u}{dx^2}} = \mathcal{D}_2^{(q)}\widehat{u}, \tag{11}$$

$$\widehat{\frac{d^3u}{dx^3}} = \mathcal{D}_1^{(q)}\widehat{\frac{d^2u}{dx^2}}, \tag{12}$$

$$\widehat{\frac{d^4u}{dx^4}} = \mathcal{D}_2^{(q)}\widehat{\frac{d^2u}{dx^2}}, \tag{13}$$

$$\widehat{\frac{d^5u}{dx^5}} = \mathcal{D}_1^{(q)}\widehat{\frac{d^4u}{dx^4}}, \tag{14}$$

$$\widehat{\frac{d^6u}{dx^6}} = \mathcal{D}_2^{(q)}\widehat{\frac{d^4u}{dx^4}}, \tag{15}$$

where superscript (q) is used to denote the order of the IRBF scheme.

Consider function $u = \sin(2\pi x)$, $0 \le x \le 1$. Let h be the grid size. We employ M uniform grids, $(h_1, h_2, \cdots, h_M)$, to represent the domain, and measure the solution accuracy in the form of relative L_2-norm for each grid as

$$N_e = \frac{\sqrt{\sum_{i=1}^{N}\left(u_i - u_i^e\right)^2}}{\sqrt{\sum_{i=1}^{N}(u_i^e)^2}}, \tag{16}$$

where N is the number of grid points, and u and u^e are the approximate and exact functions, respectively. We fit the power function $N_e = bh^m$, where m and b are the two coefficients, to the obtained data (i.e. (h_i, N_{e_i}), $i = (1, 2, \cdots, M)$). The value of m is considered here as the average of convergence. We also measure local rates of convergence defined as $(\log N_{e_i} - \log N_{e_{i-1}})/(\log h_i - \log h_{i-1})$, where i run from 2 to M. For all grids employed, we use a fixed value $a = 0.15$ for the RBF width.

2.1 Extended precision

First, the three IRBF schemes are performed with extended precision (100-digit accuracy). The domain is discretised using $N = (11, 21, \cdots, 201)$. The obtained results are shown in Figure 1.

Using IRBF2, the average rates of convergence for approximating the 1st, 2nd, 3rd, 4th, 5th and 6th derivatives are 11.76, 10.59, 9.34, 8.04, 6.54 and 5.05, respectively. Its local convergence rates are in range of 4.07 to 27.67 for the first derivative, 3.00 to 26.47 for the second derivative, 1.69 to 25.21 for the third derivative, 0.40 to 23.92 for the fourth derivative, -1.05 to 22.55 for the fifth derivative, and -0.83 to 21.11 for the sixth derivative.

Using IRBF4, the average rates of convergence for approximating the 1st, 2nd, 3rd, 4th, 5th and 6th derivatives are 13.71, 12.59, 11.39, 10.19, 8.87 and 7.48, respectively. Its local convergence rates are in range of 6.72 to 29.57 for the first derivative, 5.66 to 28.39 for the second derivative, 4.40 to 27.18 for the third derivative, 3.22 to 25.93 for the fourth derivative, 1.75 to 24.62 for the fifth derivative, and 0.23 to 23.27 for the sixth derivative.

Using IRBF6, the average rates of convergence for approximating the 1st, 2nd, 3rd, 4th, 5th and 6th derivatives are 15.76, 14.67, 13.50, 12.34, 11.09 and 9.83, respectively. Its local convergence rates are in range of 9.43 to 31.49 for the first derivative, 8.38 to 30.34 for the second derivative, 7.17 to 29.15 for the third derivative, 6.03 to 27.94 for the fourth derivative, 4.74 to 26.67 for the fifth derivative, and 3.47 to 25.38 for the sixth derivative.

These results indicate that the approximation accuracy is significantly enhanced with an increase in the order of the IRBF scheme. However, Figure 1 also shows that higher-order IRBF schemes produce larger values of the matrix condition number.

For small grid sizes (i.e. $h \leq 0.017$ or $N \geq 61$), the three IRBF schemes all produce exponential rates of convergence (with respect to grid refinement) for all the derivatives under consideration. The data form a straight line when displayed on a semilog plot whose y axis is logarithmic. For each IRBF scheme, we fit exponential functions, $Ne = K\chi^{a/h}$, to

the data of the derivative functions (Table 1). The obtained values of χ are between 0 and 1.

Figure 2 compares the condition number and approximation accuracy in the IRBF6 and conventional differentiated RBF (DRBF) schemes. Both schemes use the same RBF width ($a = 0.15$). The present IRBF6 scheme has a higher condition number but is more accurate than the DRBF scheme.

2.2 Double precision

The three IRBF schemes are implemented with double precision. The obtained results are shown in Figures **??**-3. When compared to the extended precision approach, as expected, the double-precision approach is only able to produce similar results at the first few values of N.

2.3 Mixed precision

The IRBF schemes are to be used in solving PDEs, where the discretisation involves grid lines in the x and y directions. The algebraic systems derived from discretising PDEs are typically large. In engineering practice, one does not need to have full accuracy. It is desirable to work with double precision in solving PDEs. In this regard, the case of using mixed precision is considered here. The matrices $\mathcal{D}_1$ and $\mathcal{D}_2$ in (10)-(15) are constructed with 32-digit accuracy and then converted to double precision. The original functions in (10)-(11) are evaluated in double precision. Results by the mixed-precision approach are shown in Figure 3 for IRBF6, which indicate that (i) much higher values of N (much smaller values of h) can be employed here when compared to the double-precision approach; (ii) highly-accurate results are obtained; and (iii) for a given grid size, the higher the order of the IRBF scheme the more accurate the solution will be.

Periodic conditions: For some problems, function $u(x)$ is periodic. It should be em-

phasised that the IRBF schemes allow one to impose the equal condition on values of the derivatives (up to the second order for IRBF2, the fourth order for IRBF4 and the sixth order for IRBF6) at the two end nodes in an exact manner. The imposition can be carried out in the conversion system. Taking IRBF6, for example, the matrix and vectors in the conversion system can now take the form

$$\mathcal{C} = \begin{bmatrix}
I_1^{(0)}(x_1), & \cdots, & I_{N_x}^{(0)}(x_1), & \frac{x_1^5}{5!}, & \cdots, & x_1, & 1 \\
I_1^{(0)}(x_2), & \cdots, & I_{N_x}^{(0)}(x_2), & \frac{x_2^5}{5!}, & \cdots, & x_2, & 1 \\
 & \cdots & & & \cdots & & \\
I_1^{(0)}(x_N), & \cdots, & I_N^{(0)}(x_N), & \frac{x_N^5}{5!}, & \cdots, & x_N, & 1 \\
I_1^{(1)}(x_N) - I_1^{(1)}(x_1), & \cdots, & I_N^{(1)}(x_N) - I_N^{(1)}(x_1), & \frac{x_N^4}{4!} - \frac{x_1^4}{4!}, & \cdots, & 0, & 0 \\
I_1^{(2)}(x_N) - I_1^{(2)}(x_1), & \cdots, & I_N^{(2)}(x_N) - I_N^{(2)}(x_1), & \frac{x_N^3}{3!} - \frac{x_1^3}{3!}, & \cdots, & 0, & 0 \\
I_1^{(3)}(x_N) - I_1^{(3)}(x_1), & \cdots, & I_N^{(3)}(x_N) - I_N^{(3)}(x_1), & \frac{x_N^2}{2} - \frac{x_1^2}{2}, & \cdots, & 0, & 0 \\
I_1^{(4)}(x_N) - I_1^{(4)}(x_1), & \cdots, & I_N^{(4)}(x_N) - I_N^{(4)}(x_1), & x_N - x_1, & \cdots, & 0, & 0 \\
I_1^{(5)}(x_N) - I_1^{(5)}(x_1), & \cdots, & I_N^{(5)}(x_N) - I_N^{(5)}(x_1), & 0, & \cdots, & 0, & 0 \\
I_1^{(6)}(x_N) - I_1^{(6)}(x_1), & \cdots, & I_N^{(6)}(x_N) - I_N^{(6)}(x_1), & 0, & \cdots, & 0, & 0
\end{bmatrix},$$

$$\widehat{u} = (u_1, u_2, \cdots, u_N, 0, 0, 0, 0, 0, 0)',$$

$$\widehat{w} = (w_1, w_2, \cdots, w_N, c_1, c_2, \cdots, c_6)'.$$

As shown in Figure 4, by applying the periodic boundary conditions, the levels of accuracy for all IRBF schemes are improved by several orders of magnitude, particularly for approximating high-order derivatives.

Domain decomposition: With the domain replaced with a set of overlapping subdomains, the computation becomes much more efficient as one needs to deal with smaller algebraic systems. In this work, the overlapping regions have a length of $4h$. The solution accuracy versus grid size using 2 subdomains and 4 subdomains by IRBF6 are plotted in Figure 5. When compared to the single domain results (hollow symbols), similar levels of accuracy are achieved. At small values of h, the domain decomposition approach yields slightly better accuracy. Perhaps the reasons for these are that the systems in the domain decomposition

approach are much smaller, and far-away points do not affect much the approximation qualities.

RBF width: The accuracy and stability of an IRBF solution are dependent on not only the grid size but also the RBF width. For the solution accuracy, the optimal value of the RBF width is problem-dependent. The width can take a relatively-large value for a smooth function. For the numerical stability, as shown in Figure 6, the matrix condition number is significantly reduced with a decrease in the RBF width, particularly at dense grids. It also shows that when the RBF width is reduced to 0.005, the solution is observed to be stable for all values of N considered, where the rates of grid convergence are 6.61, 5.61, 4.58, 3.49, 2.54 and 1.51 for the 1st-, 2nd, 3rd-, 4th-, 5th- and 6th-order derivatives, respectively.

3 Solving PDEs

In [1], the domain of interest, which can be non-rectangular, is discretised by means of Cartesian grids. Interior nodes are simply grid points, while boundary nodes are the intersections of the grid lines with the boundaries. At each interior node, there are two 3-point stencils constructed: one in the x direction and the other in the y direction. The interpolant on a stencil is

$$\frac{d^2u_i}{dx^2} = \eta_1 u_{i-1} + \eta_2 u_i + \eta_3 u_{i+1} + \overline{\eta}_1 \frac{d^2u_{i-1}}{dx^2} + \overline{\eta}_2 \frac{d^2u_{i+1}}{dx^2} + \cdots + \overline{\eta}_9 \frac{d^6u_{i-1}}{dx^6} + \overline{\eta}_{10} \frac{d^6u_{i+1}}{dx^6}, \quad (17)$$

which involves nodal values of not only function u but also its derivatives of orders up to 6. For simplicity, the method is described in detail for the solution of

$$\frac{\partial^2 u}{\partial x^2} + \frac{\partial^2 u}{\partial y^2} = f(x, y), \quad (18)$$

subjected to Dirichlet boundary conditions and defined on a rectangular domain that is discretised by a set of $N_x \times N_y$ points. Consider an interior node (i, j) (intersection between the ith horizontal and jth vertical grid lines). Its four neighbours are $(i-1, j)$, $(i+1, j)$,

$(i, j-1)$ $(i, j+1)$. The IRBF approximation in the x and y directions are constructed on (x_{i-1}, x_i, x_{i+1}) and (y_{j-1}, y_j, y_{j+1}), respectively by means of (17). The discretisation process leads to a set of algebraic equations:

$$\frac{\partial^2 u_{i,j}}{\partial x^2} + \frac{\partial^2 u_{i,j}}{\partial y^2} = f_{i,j}, \tag{19}$$

where $2 \leq i \leq N_x - 1$ and $2 \leq j \leq N_y - 1$. In (19), $\partial^2 u_{i,j}/\partial x^2$ is a linear function of $u_{i,j}$, $u_{i-1,j}$, $u_{i+1,j}$, $\partial^2 u_{i-1,j}/\partial x^2$, $\partial^2 u_{i+1,j}/\partial x^2$, ..., $\partial^6 u_{i-1,j}/\partial x^6$ and $\partial^6 u_{i+1,j}/\partial x^6$, and $\partial^2 u_{i,j}/\partial y^2$ a linear function of $u_{i,j}$, $u_{i,j-1}$, $u_{i,j+1}$, $\partial^2 u_{i,j-1}/\partial y^2$, $\partial^2 u_{i,j+1}/\partial y^2$, ..., $\partial^6 u_{i,j-1}/\partial y^6$ and $\partial^6 u_{i,j+1}/\partial y^6$. The nodal derivative values here are unknown, and we employ a Picard-type iteration scheme to find their values:

1. Set nodal derivatives of the 2nd, 3rd, 4th, 5th and 6th orders of u along the grid lines to zero.

2. Solve the algebraic equation set derived from (19).

3. Relax the solution

$$\text{sol}^k = \zeta \text{sol}^k + (1 - \zeta)\text{sol}^{k-1}, \tag{20}$$

   where subscript k denotes a current iteration, "sol" a vector containing interior nodal values of u, and ζ a relax factor $(0 < \zeta \leq 1)$.

4. Compute the derivatives using IRBF2/IRBF4/IRBF6.

5. Compute Convergence Measure defined as

$$CM = \frac{\text{norm}(\text{sol}^k - \text{sol}^{k-1})}{\text{norm}(\text{sol}^k)}. \tag{21}$$

6. Check CM. If CM is less than a specified tolerance, stop the iteration and output the result. Otherwise, repeat from Step 2.

RBF width: In solving PDEs, we investigate two cases: a fixed width and a linearly-variable width that can be described in the following single function

$$a = \beta(h - h_{min}) + \bar{a}, \tag{22}$$

where $\bar{a}$ is a fixed width, h_{min} the smallest grid size used, β a chosen constant controlling the rate of change of the RBF width with respect to the grid size. Value of β is zero for the fixed-width case and non-zero for the variable-width case. The two width cases have the same value at $h = h_{min}$. It is recommended that one can choose $\bar{a}$ where the IRBF approximations at $h = h_{min}$ are still stable. With 32-digit accuracy employed here, for an accurate and stable solution, the condition number of the conversion matrix can be in range of 10^{15} to 10^{32}, which means that the fixed width $\bar{a}$ can be selected from a wide range of values.

Problems with slow-variation solutions: it is known that the optimal width here takes a relatively-large value at which the coefficient matrix is highly ill-conditioned. As shown in Section 2 (IRBFs for approximating a smooth function and its derivatives), exponential convergence results are obtained at small values of the grid size h. At larger values of h, the matrix condition number is lower and it is possible to employ larger values of the RBF width to achieve better accuracy. With $\beta > 0$, values of a are larger at coarse grids than at fine grids. Positive values of β can thus be used effectively to improve the level of accuracy at coarse grids.

Problems with rapid-variation solutions: values of the RBF width to be used here should be smaller in order to capture rapid changes in the solutions. It can be seen that the RBF approximations at coarse grids using relatively-large widths are not be able to capture the rapid-variation solutions. With $\beta < 0$, values of a are smaller at coarse grids than at fine grids. Negative values of β can thus be used effectively to improve the level of accuracy at coarse grids.

3.1 Problems with slow-variation solutions

Consider Poisson equation with the RHS given by

$$f(x,y) = 4(1-\pi^2)\sin(2\pi x)\sinh(2y) + 16(1-\pi^2)\cosh(4x)\cos(4\pi y), \tag{23}$$

and the domain of interest: $-1/2 \leq x, y \leq 1/2$. The exact solution to this problem is

$$u^{(e)}(x,y) = \sin(2\pi x)\sinh(2y) + \cosh(4x)\cos(4\pi y),$$

from which boundary values of u can be derived. It can be seen that the solution is a smooth function.

We choose $h_{min} = 1/150$. The domain is discretised using $N_x = N_y = (11, 13, \cdots, 151)$. Results concerning the effects of the RBF width on (i) the condition number of the conversion matrix, denoted by $cond(C)$, in the process of approximating function u and its derivatives on the grid lines, (ii) the condition number of the system matrix, denoted by $cond(A)$, in the process of solving the PDE, and (iii) the solution accuracy, denoted by N_e, are shown in Figure 7 for IRBF2, Figure 10 for IRBF4 and Figure 12 for IRBF6.

It can be seen that for all IRBF schemes, the growths of the matrix condition number with respect to grid refinement are low for the system matrices (rates of about 2) and high for the conversion matrices. The RBF width has a strong effect on the condition number of the conversion matrix, but has no effect on the condition number of the system matrix. The condition number is high for the conversion matrix (and thus there is the need for using extended precision here) and low for the system matrix (and thus one can use double precision here). Reducing the RBF width significantly improves the condition number for the conversion matrix particularly at fine grids. The figures also include results for the fixed- and variable-width cases, which are discussed in detail next.

IRBF2: The parameters in (22) are chosen as

$$h_{min} = 1/150, \quad \bar{a} = (0.05, 0.06, 0.07, 0.08), \quad \beta = (0, 4).$$

In terms of h_{min}, $\bar{a} = (7.5, 9.0, 10.5, 12)h_{min}$. It can be seen that the errors reduce quick for both fixed ($\beta = 0$) and variable ($\beta > 0$) width cases. Figure 8 shows the convergence of the solution with respect to grid refinement for ($\beta = 0, \bar{a} = 0.08$) and ($\beta = 4, \bar{a} = 0.08$). The case of $\beta > 0$ yields higher degrees of accuracy but a slower average rate of convergence than the case of $\beta = 0$. It can also seen that the IRBF approximations using any value of β between 0 and 4 also produce very good results. Figure 9 shows a comparison of convergence rates for the variable-width case. The average rates of convergence are $O(h^{4.56})$ for $a = 0.05$, $O(h^{4.94})$ for $a = 0.06$, $O(h^{5.33})$ for $a = 0.07$ and $O(h^{5.74})$ for $a = 0.08$.

IRBF4: The parameters in (22) are chosen as

$$h_{min} = 1/150, \quad (\bar{a}, \beta) = [(2h_{min}, 2), (3h_{min}, 3), (4h_{min}, 4), (5h_{min}, 5)].$$

With these choices, the variable width is simply computed as $a = \beta h$, where $\beta = (2, 3, 4, 5)$. Similar remarks can also be made here. Figure 11 shows a comparison of convergence rates for the variable-width case. The average rates of convergence are $O(h^{5.66})$ for $\beta = 2$, $O(h^{5.77})$ for $\beta = 3$, $O(h^{5.87})$ for $\beta = 4$ and $O(h^{5.84})$ for $\beta = 5$.

IRBF6: The parameters in (22) are chosen as

$$h_{min} = 1/150, \quad (\bar{a}, \beta) = [(2h_{min}, 2), (3h_{min}, 3), (4h_{min}, 4), (5h_{min}, 5)].$$

With these choices, the variable width is simply computed as $a = \beta h$, where $\beta = (2, 3, 4, 5)$. Similar remarks can also be made here. Figure 13 shows a comparison of convergence rates for the variable-width case. For the first 16 values of N_x and N_y (i.e. $N_x = N_y = (11, 13, \cdots, 41)$), the solution converges as $O(h^{7.74})$ for $\beta = 2$, $O(h^{8.54})$ for $\beta = 3$, $O(h^{8.98})$ for $\beta = 4$ and $O(h^{9.38})$ for $\beta = 5$. As expected, with a tolerance of 10^{-10} used in the

Picard-type iteration scheme, the solution accuracy will not further decrease at fine grids.

Figure 14 compares the solution accuracies of the IRBF schemes employed with their largest widths. The larger the order of the IRBF scheme, the more accurate the solution will be.

4 Problems with rapid-variation solutions

Consider the following convection-diffusion equation

$$-\varepsilon\left(\frac{\partial^2 u}{\partial x^2}+\frac{\partial^2 u}{\partial y^2}\right)+\frac{\partial u}{\partial x}=0, \tag{24}$$

defined on the domain $(0,1)\times(0,1)$ and subjected to

$$u(x,0)=0, \quad 0\le x\le 1, \tag{25}$$

$$u(x,1)=0, \quad 0\le x\le 1, \tag{26}$$

$$u(0,y)=\sin(\pi y), \quad 0\le y\le 1, \tag{27}$$

$$u(1,y)=\sin(2\pi y), \quad 0\le y\le 1. \tag{28}$$

The exact solution to this problem is

$$u_e(x,y)=\exp(Rx/2)\sin(\pi y)\left[2\exp(-R/2)\sinh(\sigma x)+\sinh(\sigma(1-x))\right]/\sinh(\sigma), \tag{29}$$

where $R=1/\varepsilon$ and $\sigma=\sqrt{\pi^2+R^2/4}$.

When $\varepsilon \ll 1$, the problem is convection-dominated, and numerical simulation becomes difficult due to the presence of a regular boundary layer along the downstream edge $x=1$ (Figure 15). Several numerical schemes for overcoming these difficulties have been proposed. Most of them are based on upwind differencing of the convective terms. If the diffusion term is approximated by central differences and the convection terms by suitable forward or backward differences, the resultant scheme is called the original upwind scheme or the

UDS. Note that the UDS is of only first-order accuracy and can cause a false diffusion. To maintain high levels of accuracy of the IRBF solution, we employ the upwind scheme in conjunction with the deferred-correction strategy

$$\left(\frac{\partial u_{i,j}}{\partial x}\right)^k = \left(\frac{u_{i,j} - u_{i-1,j}}{h}\right)^k + \Delta^k, \tag{30}$$

where k denotes a current iteration and Δ is the correction term defined as

$$\Delta^k = \left(\frac{u_{i,j} - u_{i-1,j}}{h}\right)^{k-1} + \left(\frac{\partial u_{i,j}}{\partial x}\right)^{k-1}, \tag{31}$$

where the last term on the right site is computed using the proposed high-order IRBF schemes.

This problem has been studied in [27,28]. As in [28], we choose $h_{min} = 1/64$. Table 2 shows results by the upstream IRBF2 scheme (with and without using the deferred-correction strategy) and the UDS. It is clear that utilisation of the deferred-correction strategy helps maintain a high level of the IRBF solution in simulating convection-dominated flows.

To compare with those reported in [28], we measure the solution accuracy in the form of average relative errors, and consider $\varepsilon = 0.01$. The domain is discretised using $N_x = N_y = (33, 37, \cdots, 65)$. Results concerning the effects of the RBF width on (i) the condition number of the conversion matrix, (ii) the condition number of the system matrix, and (iii) the solution accuracy, denoted by average RE, are shown in Figure 16 for IRBF2 and Figure 18 for IRBF6.

It can be seen that for all IRBF schemes, the growths of the matrix condition number with respect to grid refinement are low for the system matrices (rates of about 2) and high for the conversion matrices. The RBF width has a strong effect on the condition number of the conversion matrix, but has no effect on the condition number of the system matrix. Reducing the RBF width significantly improves the condition number for the conversion matrix particularly at fine grids. The figures also include results for the fixed- and variable-width cases, which are discussed in detail next.

IRBF2: The parameters in (22) are chosen as

$$h_{min} = 1/64, \quad \bar{a} = 0.15, \quad \beta = (0, -5)$$

It can be seen that the errors reduce quick for both fixed ($\beta = 0$) and variable ($\beta < 0$) width cases. Figure 17 shows the convergence of the solution with respect to grid refinement for the two RBF-width cases. The case of $\beta < 0$ yields higher degrees of accuracy but a slower average rate of convergence than the case of $\beta = 0$. The average rates of convergence are $O(h^{6.03})$ for the fixed width and $O(h^{4.39})$ for the variable width.

IRBF6: The parameters in (22) are chosen as

$$h_{min} = 1/64, \quad \bar{a} = 0.1, \quad \beta = (0, -5)$$

Figure 19 shows a comparison of convergence rates for the two RBF-width cases. Similar remarks can also be made here. The average rates of convergence are $O(h^{6.83})$ for the fixed width and $O(h^{5.05})$ for the variable width.

Figure 20 compares the solution accuracy between the central difference (CD), discrete weighted mean approximation (DWMA) and IRBF6 schemes. The three schemes are all based on local stencils of 5 points. For a wide range of the RBF width employed, the proposed scheme yields the most accurate results. Note that results by the CD and DWMA schemes are extracted from [28].

Higher-order IRBF schemes produce higher levels of the solution accuracy and larger condition numbers for the conversion matrices. In the case of problems whose solutions are highly oscillating functions, a large number of nodes should be employed for an accurate simulation. In this situation, the use of lower-order IRBF schemes and smaller values of β is preferable.

5 Concluding remarks

In this work, several effective schemes of computing high-order derivatives along a grid line are reported. It is shown that (i) an exponential rate of convergence is achieved by using integrated RBFs and extended precision, and (ii) their computational efficiencies are improved by using overlapping domain decomposition and mixed-precision calculations. The use of the proposed IRBF approximation schemes in solving PDEs is discussed in detail. Two different ways of choosing the RBF width, namely fixed and variable values with respect to grid refinement, are implemented in a simple framework. For the latter, the RBF width is chosen as a linear function of the grid size. Both positive and negative values of the slope are studied. Positive values can be used effectively for problems with slow-variation solutions, while negative values can be used effectively for problems with rapid-variation solutions. The case of using a variable width can yield better accuracy at coarser grids than the case of using a fixed width. For the convection-diffusion equations, the proposed approximation schemes can effectively be utilised in conjunction with a deferred-correction strategy to obtain an accurate solution in simulating convection-dominated flows.

References

1. Mai-Duy N, Strunin D. New approximations for one-dimensional 3-point and two-dimensional 5-point compact integrated RBF stencils. Engineering Analysis with Boundary Elements 2021;125:12-22.

2. Canuto C, Hussaini MY, Quarteroni A, Zang TA. Spectral Methods in Fluid Dynamics. Berlin: Springer-Verlag; 1988.

3. Hirsh RS. Higher order accurate difference solutions of fluid mechanics problems by a compact differencing technique. Journal of Computational Physics 1975;19(1):90-109.

4. Kansa EJ. Multiquadrics - A scattered data approximation scheme with applications to computational fluid-dynamics - II. Solutions to parabolic, hyperbolic and elliptic partial

differential equations. Computers & Mathematics with Applications 1990;19(8/9):147-161.

5. Mai-Duy N, Tanner RI. Computing non-Newtonian fluid flow with radial basis function networks. International journal for numerical methods in fluids 2005;48(12):1309-1336;

6. Mai-Duy N, Tran-Cong T, Integrated radial-basis-function networks for computing Newtonian and non-Newtonian fluid flows. Computers and Structures 2009;87(11-12):642-650.

7. Jankowska MA, Karageorghis A. Variable shape parameter Kansa RBF method for the solution of nonlinear boundary value problems. Engineering Analysis with Boundary Elements 2019;103:32-40.

8. Liu C, Han X, Zhang L. Unconditional convergence of iterative approximation methods. Engineering Analysis with Boundary Elements 2021;126:161-168.

9. Zeng Y, Duan Y, Liu B-S. Solving 2D parabolic equations by using time parareal coupling with meshless collocation RBFs methods. Engineering Analysis with Boundary Elements 2021;127:102-112.

10. Shu C, Ding H, Yeo KS. Local radial basis function-based differential quadraturemethod and its application to solve two-dimensional incompressible Navier-Stokes equations. Comput. Methods Appl. Mech. Engrg. 2003;192:941-954.

11. Harris MF, Kassab AJ, Divo E. A shock-capturing meshless scheme using RBF blended interpolation and moving least squares. Engineering Analysis with Boundary Elements 2019;109:81-93.

12. Safarpoor M, Shirzadi A. A localized RBF-MLPG method for numerical study of heat and mass transfer equations in elliptic fins. Engineering Analysis with Boundary Elements 2019;98:35-45.

13. Dehghan M, Mohammadi V. Two-dimensional simulation of the damped Kuramoto-Sivashinsky equation via radial basis function-generated finite difference scheme com-

bined with an exponential time discretization. Engineering Analysis with Boundary Elements 2019;107:168-184.

14. Mramor K, Vertnik R, Sarler B. Application of the local RBF collocation method to natural convection in a 3D cavity influenced by a magnetic field. Engineering Analysis with Boundary Elements 2020;116:1-13.

15. Tolstykh AI, Shirobokov DA. On using radial basis functions in a "finite difference mode" with applications to elasticity problems. Computational Mechanics 2003;33(1):68-79.

16. Wright GB, Fornberg B. Scattered node compact finite difference-type formulas generated from radial basis functions. Journal of Computational Physics 2006;212(1):99-123.

17. Mai-Duy N, Tran-Cong T. Compact local integrated-RBF approximations for second-order elliptic differential problems. Journal of Computational Physics 2011;230(12):4772-4794.

18. Mai-Duy N, Tran-Cong T. A compact five-point stencil based on integrated RBFs for 2D second-order differential problems. Journal of Computational Physics 2013;235:302-321.

19. Mai-Duy N, Le TTV, Tien CMT, Ngo-Cong D, Tran-Cong T. Compact approximation stencils based on integrated flat radial basis functions. Engineering Analysis with Boundary Elements 2017;74:79-87.

20. Mai-Duy N, Dalal D, Le TTV, Ngo-Cong D, Tran-Cong T. A symmetric integrated radial basis function method for solving differential equations. Numerical Methods for Partial Differential Equations 2018;34(3):959-981.

21. Le TTV, Mai-Duy N, Le-Cao K, Tran-Cong T. A time discretization scheme based on integrated radial basis functions for heat transfer and fluid flow problems. Numerical Heat Transfer, Part B: Fundamentals 2018;74(2):498-518.

22. Bhanot RP, Strunin DV, and Ngo-Cong D, Numerical solution of a highly nonlinear and non-integrable equation using integrated radial basis function network method. Chaos: An Interdisciplinary Journal of Nonlinear Science 2020;30:083119.

23. Cheng AH-D. Multiquadric and its shape parameter-A numerical investigation of error estimate, condition number, and round-off error by arbitrary precision computation. Engineering Analysis with Boundary Elements 2012;36(2):220-239.

24. Huang C-S, Lee C-F, Cheng AH-D. Error estimate, optimal shape factor, and high precision computation of multiquadric collocation method. Engineering Analysis with Boundary Elements 2007;31(7):614-623.

25. Sarra SA. Radial basis function approximation methods with extended precision floating point arithmetic. Engineering Analysis with Boundary Elements 2011;35(1):68-76.

26. Khosla PK, Rubin SG. A diagonally dominant second-order accurate implicit scheme. Computers and Fluids 1974;2(2):207-209.

27. Gartland EC. Discrete weighted mean approximation of a model convection-diffusion equation. SIAM J. Sci. Stat. Comput. 1982;3(4):460-472.

28. Gupta MM, Manohar RP, Stephenson JW. A single cell high order scheme for the convection-diffusion equation with variable coefficients. Int. J. Numer. Meth. Fluids 1984;4(7):641-651.

Table 1: Derivative approximations, $N = (61, 63, \cdots, 201)$, $a = 0.15$, extended precision (full accuracy): The coefficients of exponential functions, $Ne = K\chi^{a/h}$, used to represent the data collected from the IRBF approximations of the derivative functions. It can be seen that $0 < \chi < 1$. Note that $\alpha(\gamma)$ means $\alpha \times 10^{\gamma}$.

Derivatives	χ	K
	IRBF2	
1st	0.3727	5.8514(-4)
2nd	0.3980	2.1689(-2)
3rd	0.4264	5.0973(-1)
4th	0.4582	8.7532(+0)
5th	0.4956	1.0346(+2)
6th	0.5399	8.7663(+2)
	IRBF4	
1st	0.3358	4.4347(-6)
2nd	0.3579	1.8119(-4)
3rd	0.3823	4.7662(-3)
4th	0.4091	9.5545(-2)
5th	0.4398	1.4120(+0)
6th	0.4743	1.6678(+1)
	IRBF6	
1st	0.3019	3.6286(-8)
2nd	0.3212	1.5915(-6)
3rd	0.3426	4.5375(-5)
4th	0.3657	1.0121(-3)
5th	0.3917	1.7278(-2)
6th	0.4203	2.4779(-1)

Table 2: Convection-diffusion equation, mixed precision, IRBF2, $N_x = N_y = 65$, $\bar{a} = 0.125$, $\beta = 0$: comparison of the solution accuracy N_e between the upstream IRBF2 scheme (with and without using the deferred-correction strategy) and the UDS. Note that $\alpha(\gamma)$ means $\alpha \times 10^{\gamma}$.

		Upwind IRBF2	
ε	UDS	without correction	with correction
1/10	2.03(-2)	1.98(-2)	1.16(-6)
1/20	2.41(-2)	2.30(-2)	8.01(-6)
1/40	2.70(-2)	2.51(-2)	6.83(-5)
1/100	3.00(-2)	2.68(-2)	8.83(-4)

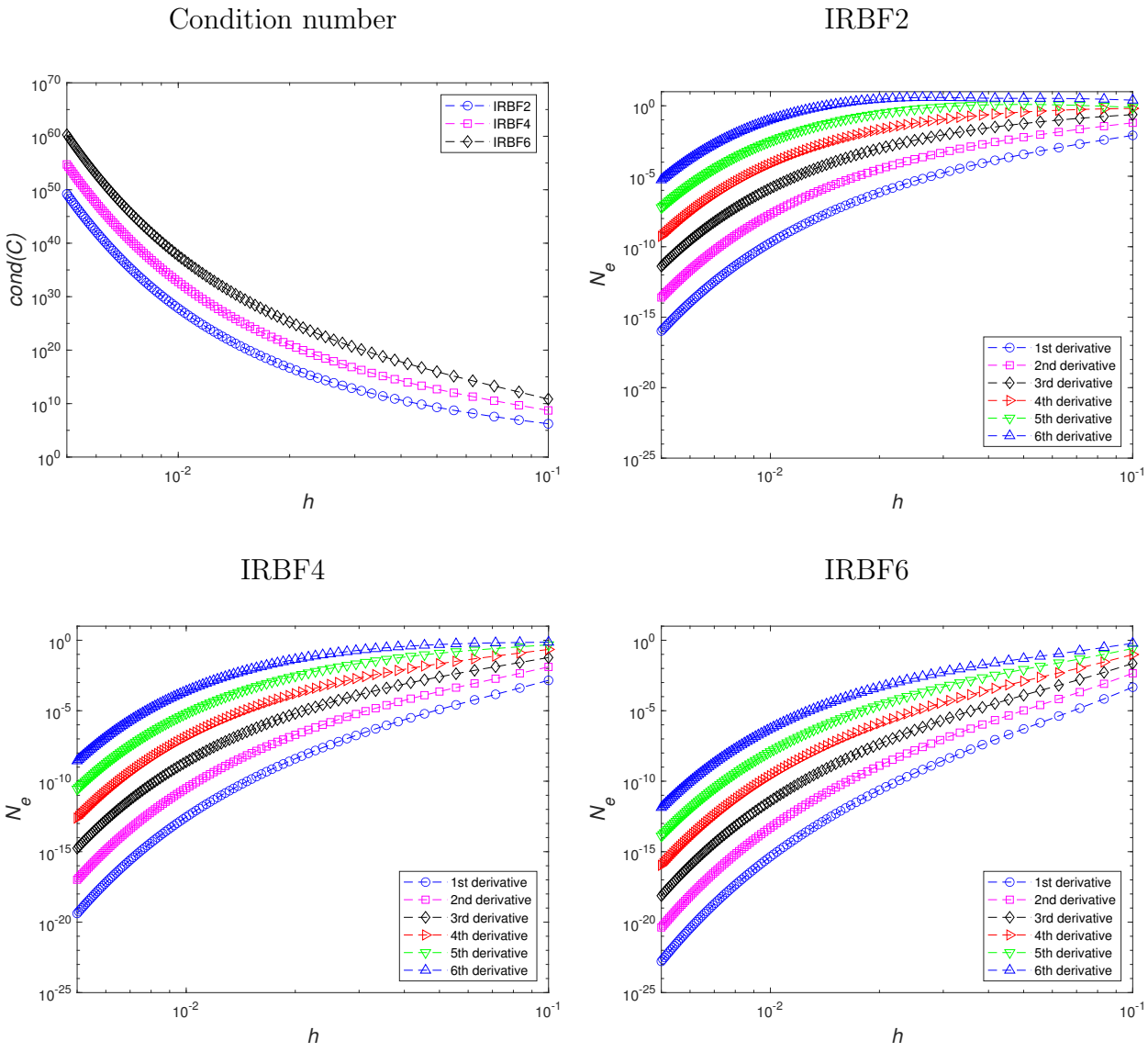

Figure 1: Derivative approximations, $N = (11, 13, \cdots, 201)$, $a = 0.15$, extended precision (full accuracy): Matrix condition number and accuracy versus grid size produced by IRBF2, IRBF4 and IRBF6. For accuracy, the same axis scales are used. It can be seen that (i) the errors by the 3 IRBF schemes decrease very rapidly when $h \leq 0.017$ or $N \geq 61$, and (ii) an IRBF scheme of higher order yields greater accuracy.

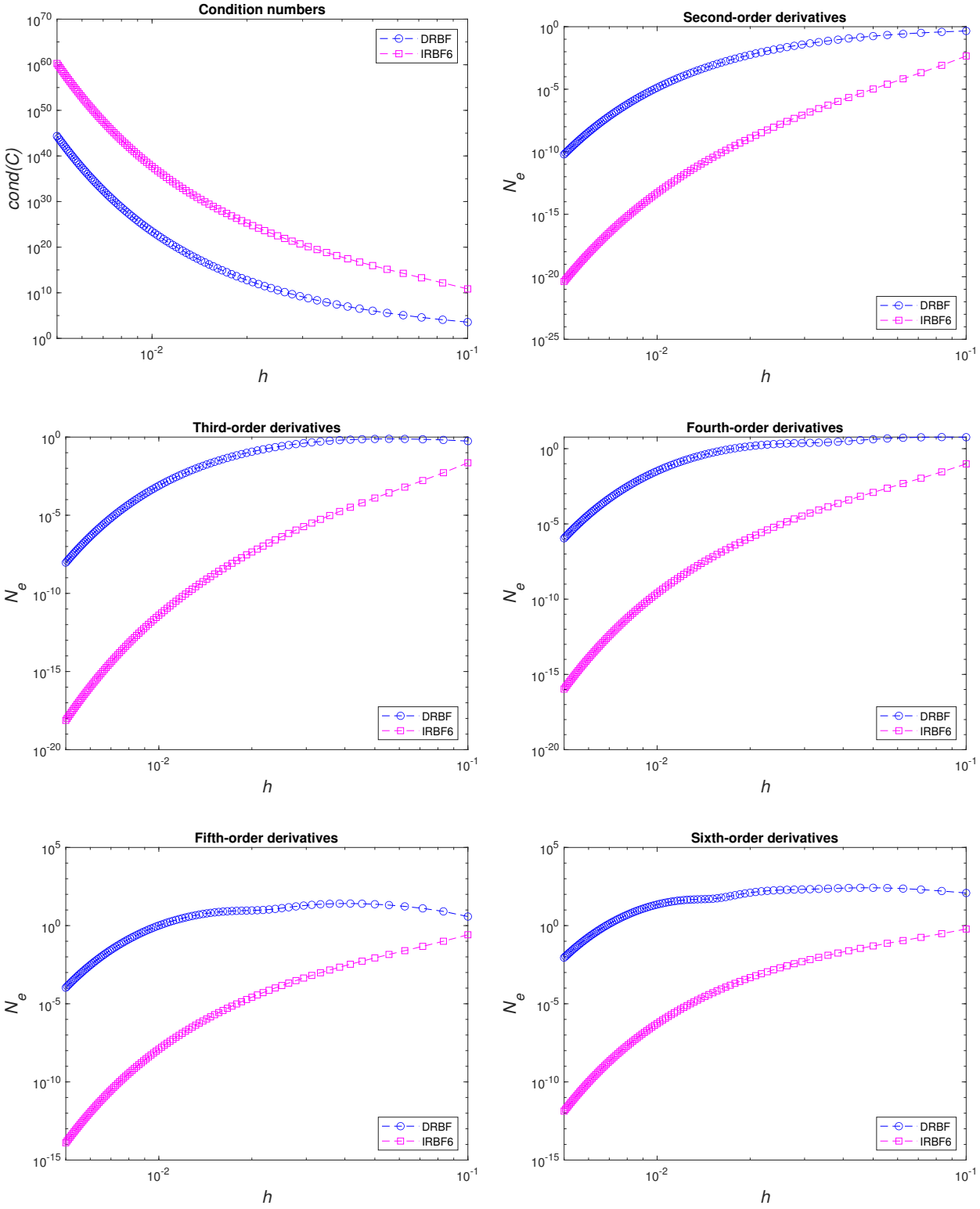

Figure 2: Derivative approximations, $N = (11, 13, \cdots, 201)$: Comparison of the condition number and accuracy in the differentiated RBF and integrated IRBF schemes that use the same width ($a = 0.15$). The latter has a larger condition number but is more accurate than the former.

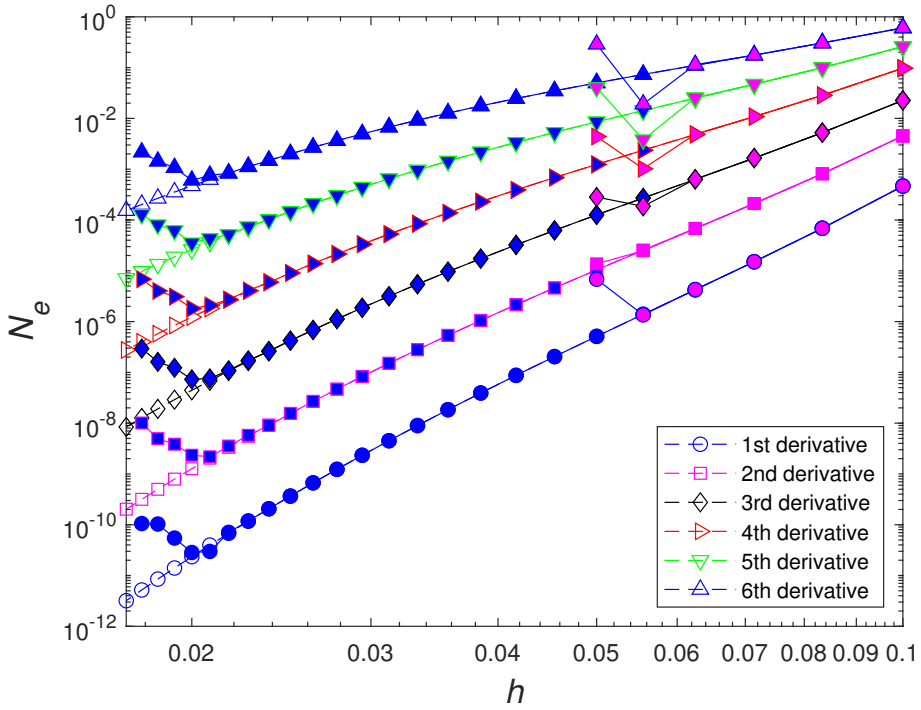

Figure 3: Derivative approximations, $a = 0.15$: Accuracy versus grid size by IRBF6 implemented with double precision (magenta solid symbols) and mixed precision (blue solid symbols). Results by the extended precision approach (hollow symbols) are also included to produce the base for comparison purposes. It can be seen that the double-precision implementation can produce similar results for N from 11 to 17, and the mixed-precision implementation can produce similar results for N from 11 to 49.

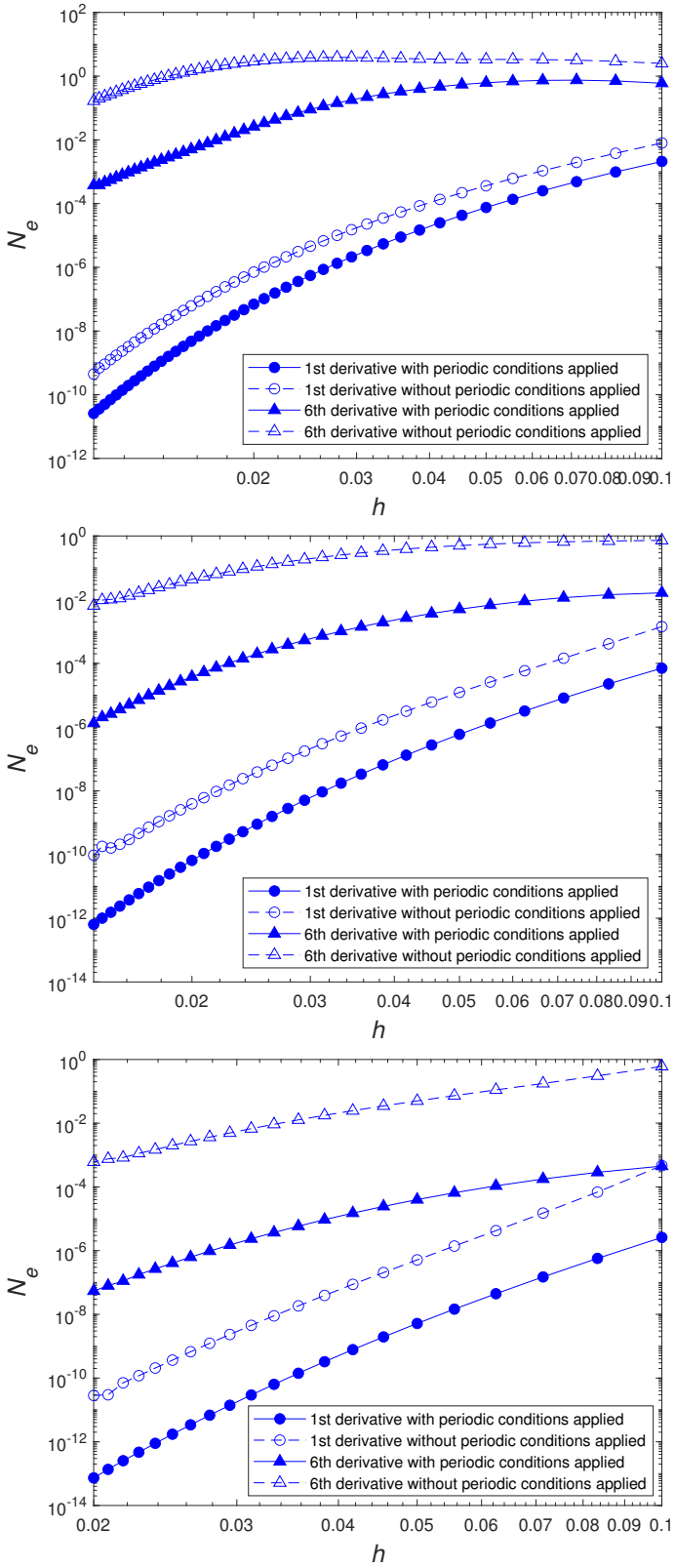

Figure 4: Derivative approximations, mixed precision: Comparisons of accuracy between two cases: with and without imposition of periodic conditions by IRBF2 (top), IRBF4 (middle) and IRBF6 (bottom). By applying the periodic boundary conditions, the levels of accuracy are improved by several orders of magnitude, particularly for high-order derivatives.

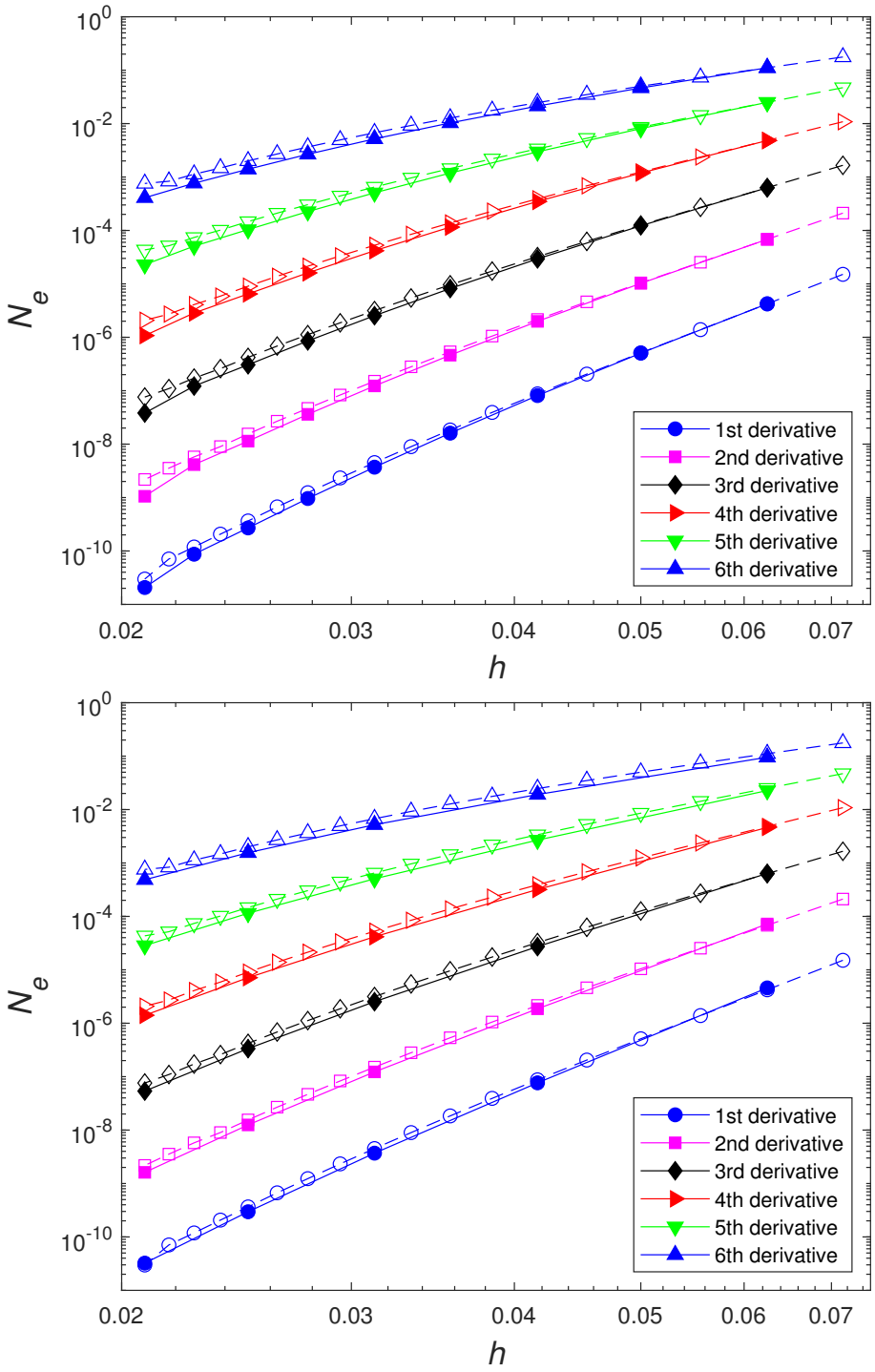

Figure 5: Derivative approximations, $a = 0.15$, mixed precision: Accuracy versus grid size by IRBF6 using 2 subdomains (top) and 4 subdomains (bottom). When compared to the single domain results (hollow symbols), slightly-better accuracy is achieved at small values of h, probably due to the fact that the systems in the domain decomposition approach are smaller. Note that the domain decomposition approach is much more efficient than the single domain approach.

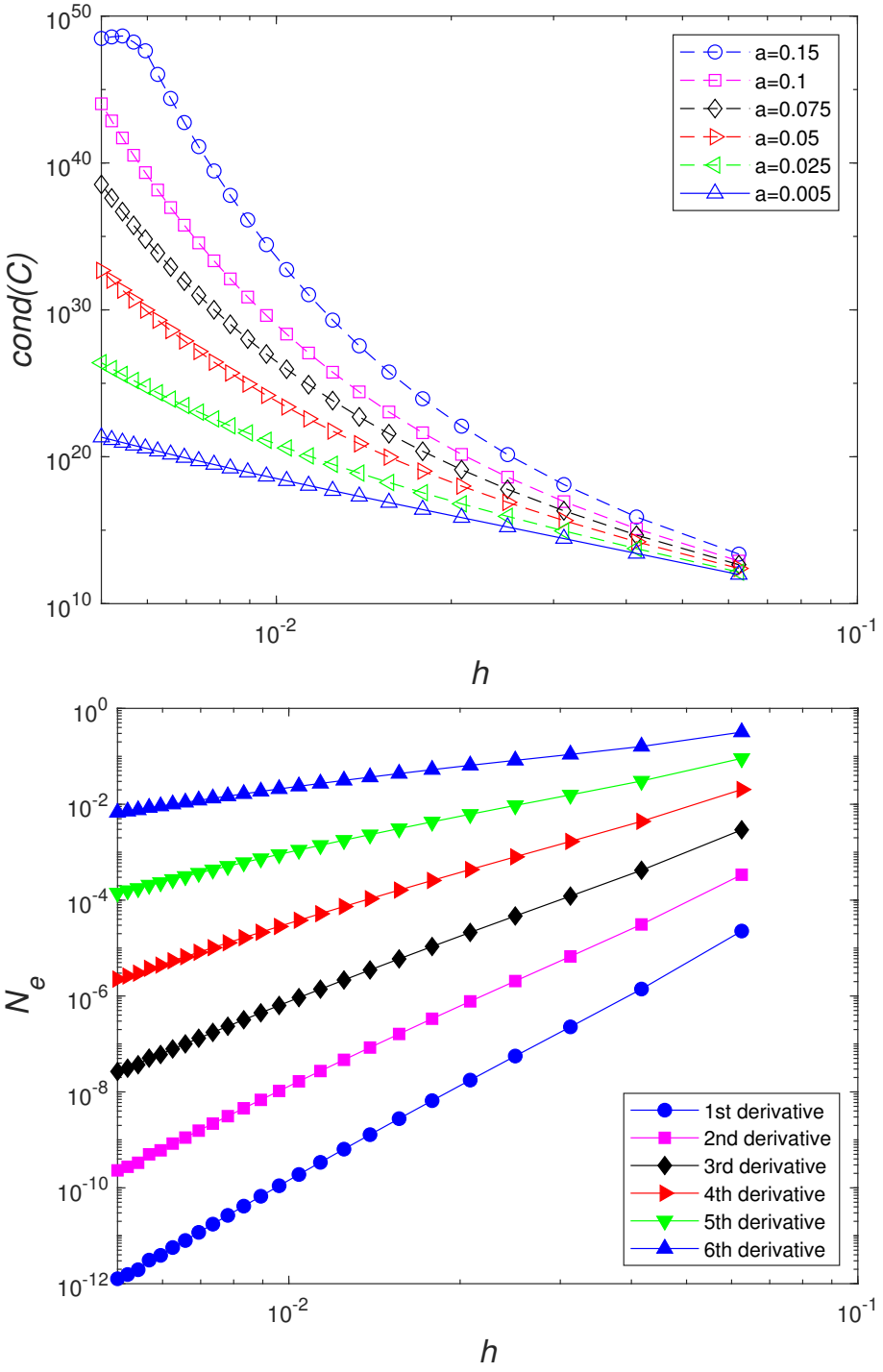

Figure 6: Derivative approximations, mixed precision, 4 subdomains, IRBF6: The matrix condition number is significantly improved with a decrease in the RBF width particularly at dense grids (top), and when the RBF width a is reduced to 0.005, the solution is observed to be stable for all values of N considered (bottom).

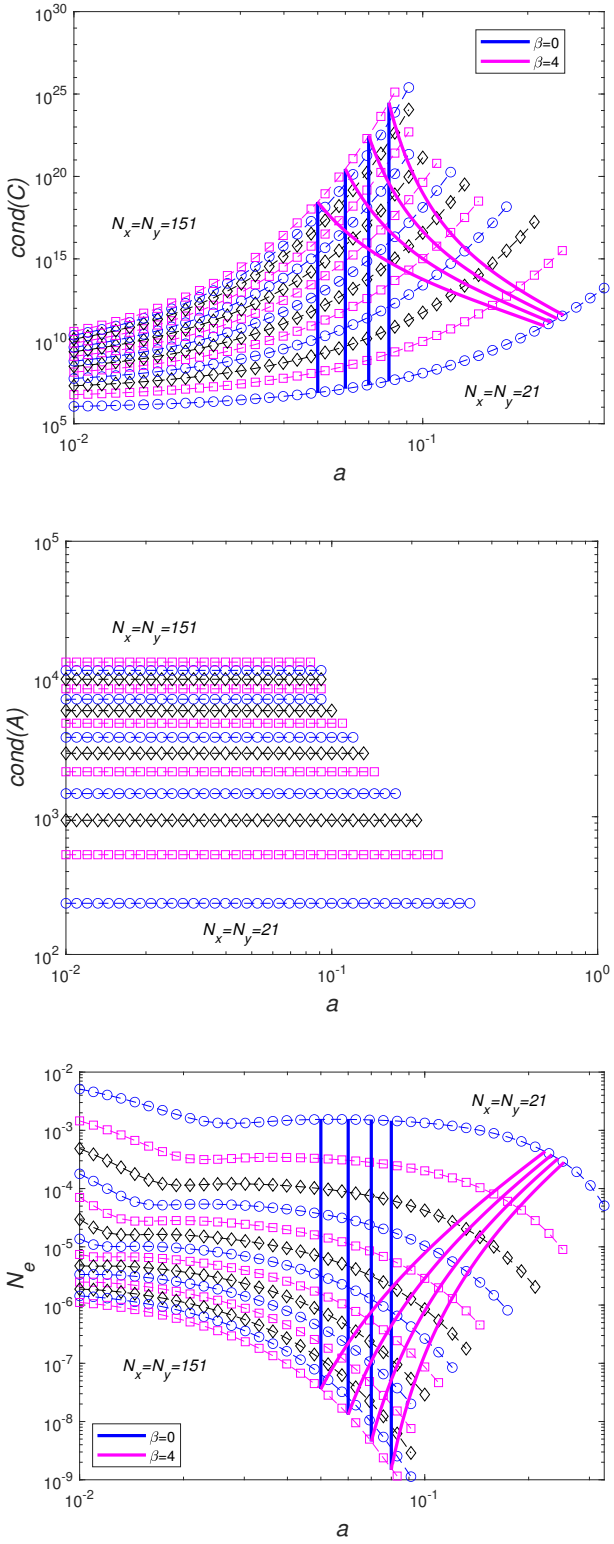

Figure 7: Poisson equation, mixed precision, IRBF2, $N_x = N_y = (21, 31, \cdots, 151)$: Plots of the matrix condition numbers and the solution accuracy versus the RBF width for several grid sizes. For a given grid size, the RBF width has a strong effect on the condition number of the conversion matrix and no effect on the condition number of the system matrix. The condition number is high for the conversion matrix and low for the system matrix. Results by two different ways of implementing the RBF width, fixed ($\bar{a} = (0.05, 0.06, 0.07, 0.08)$, $\beta = 0$) and variable ($\bar{a} = (0.05, 0.06, 0.07, 0.08)$, $\beta = 4$) values with grid refinement, are also included. The variable-width case generally yields more accurate results than the fixed-width case.

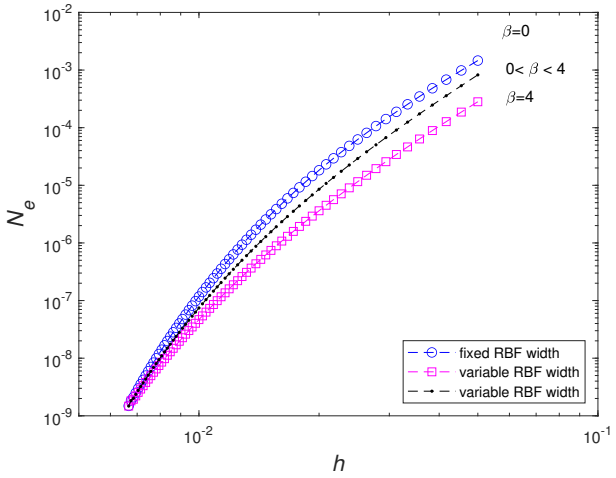

Figure 8: Poisson equation, mixed precision, IRBF2, $N_x = N_y = (11, 13, \cdots, 151)$, $0 \leq \beta = 4 \leq 4$, $\bar{a} = 0.008$: Plots of the solution accuracy versus grid size for the fixed ($\beta = 0$) and variable ($\beta = 4$) width cases. The errors reduce quick for both cases. The latter yields higher levels of accuracy but a slower average rate of convergence than the former. It can be seen that the proposed method using any β between 0 and 4 can also produce very good results.

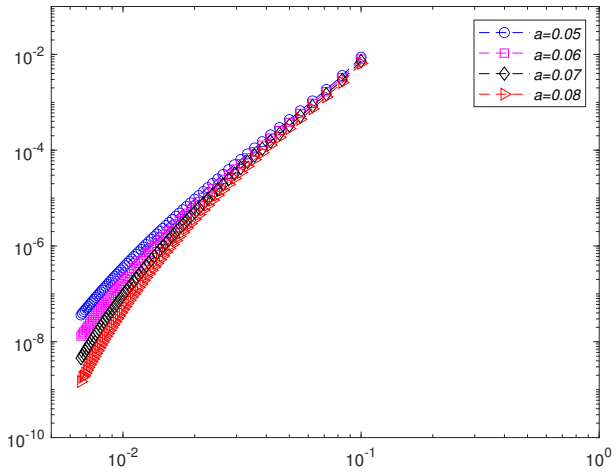

Figure 9: Poisson equation, mixed precision, IRBF2, $N_x = N_y = (11, 13, \cdots, 151)$, $\beta = 4$: Plots of the solution accuracy versus grid size for four different values of $\bar{a}$ for the fixed-width case ($\beta = 0$). The solution converges as $O(h^{4.56})$ for $a = \bar{a} = 0.05$, $O(h^{4.94})$ for $a = \bar{a} = 0.06$, $O(h^{5.33})$ for $a = \bar{a} = 0.07$ and $O(h^{5.74})$ for $a = \bar{a} = 0.08$.

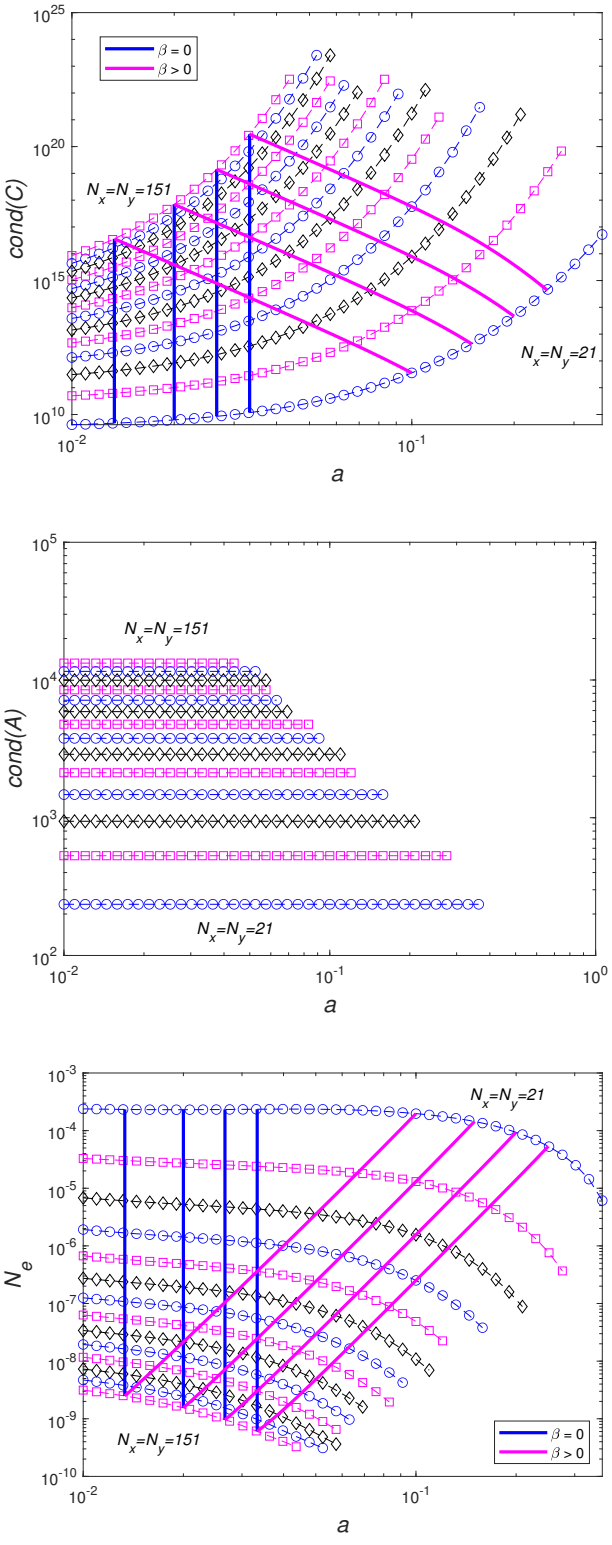

Figure 10: Poisson equation, mixed precision, IRBF4, $N_x = N_y = (21, 31, \cdots, 151)$: Plots of the matrix condition numbers and the solution accuracy versus the RBF width for several grid sizes. For a given grid size, the RBF width has a strong effect on the condition number of the conversion matrix and no effect on the condition number of the system matrix. The condition number is high for the conversion matrix and low for the system matrix. Results by two different ways of implementing the RBF width, fixed ($\bar{a} = (2h_{min}, 3h_{min}, 4h_{min}, 5h_{min})$, $\beta = 0$) and variable ($\bar{a} = \beta h_{min}$, $\beta = (2, 3, 4, 5)$) values with grid refinement, are also included. The variable-width case generally yields more accurate results than the fixed-width case.

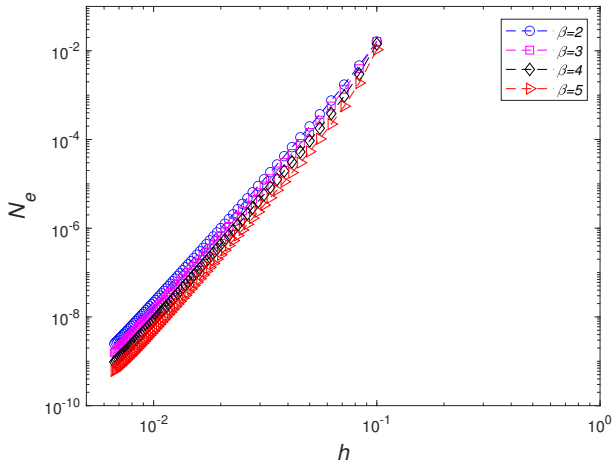

Figure 11: Poisson equation, mixed precision, IRBF4, $N_x = N_y = (11, 13, \cdots, 151)$, $\bar{a} = \beta h_{min}$, $a = \beta h$: Plots of the solution accuracy versus grid size for four different values of β for the variable-width case. The solution converges as $O(h^{5.66})$ for $\beta = 2$, $O(h^{5.77})$ for $\beta = 3$, $O(h^{5.83})$ for $\beta = 4$ and $O(h^{5.84})$ for $\beta = 5$.

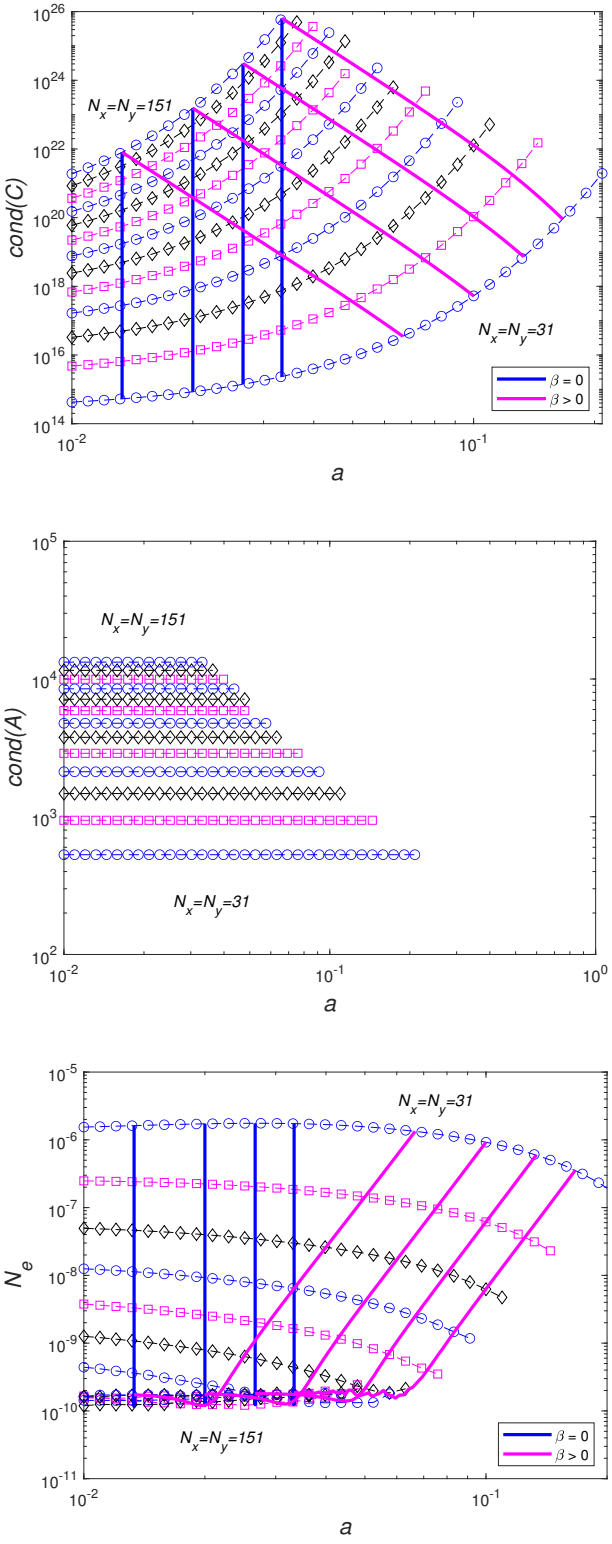

Figure 12: Poisson equation, mixed precision, IRBF6, $N_x = N_y = (31, 41, \cdots, 151)$: Plots of the matrix condition numbers and the solution accuracy versus the RBF width for several grid sizes. For a given grid size, the RBF width has a strong effect on the condition number of the conversion matrix and no effect on the condition number of the system matrix. The condition number is high for the conversion matrix and low for the system matrix. Results by two different ways of implementing the RBF width, fixed ($\bar{a} = (2h_{min}, 3h_{min}, 4h_{min}, 5h_{min})$, $\beta = 0$) and variable ($\bar{a} = \beta h_{min}$, $\beta = (2, 3, 4, 5)$) values with grid refinement, are also included. The variable-width case generally yields more accurate results than the fixed-width case.

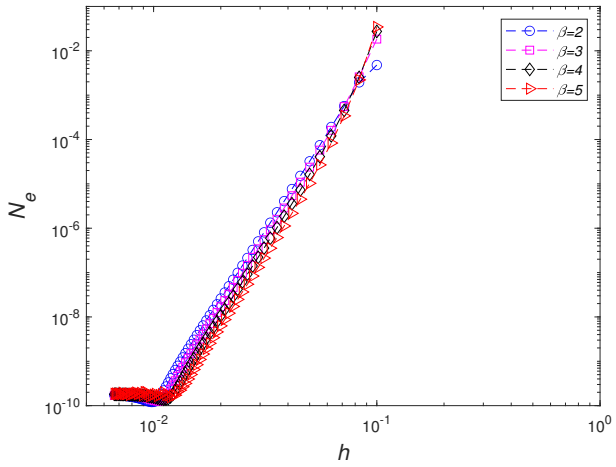

Figure 13: Poisson equation, mixed precision, IRBF6, $N_x = N_y = (11, 13, \cdots, 151)$, $\bar{a} = \beta h_{min}$, $a = \beta h$: Plots of the solution accuracy versus grid size for four different values of β for the variable-width case. The solution converges as $O(h^{7.74})$ for $\beta = 2$, $O(h^{8.54})$ for $\beta = 3$, $O(h^{8.98})$ for $\beta = 4$ and $O(h^{9.38})$ for $\beta = 5$ for the first 16 values of N_x and N_y (i.e. $N_x = N_y = (11, 13, \cdots, 41)$). As expected, with a tolerance of 10^{-10} used in the Picard-type iteration scheme, the solution accuracy will not further decrease at fine grids.

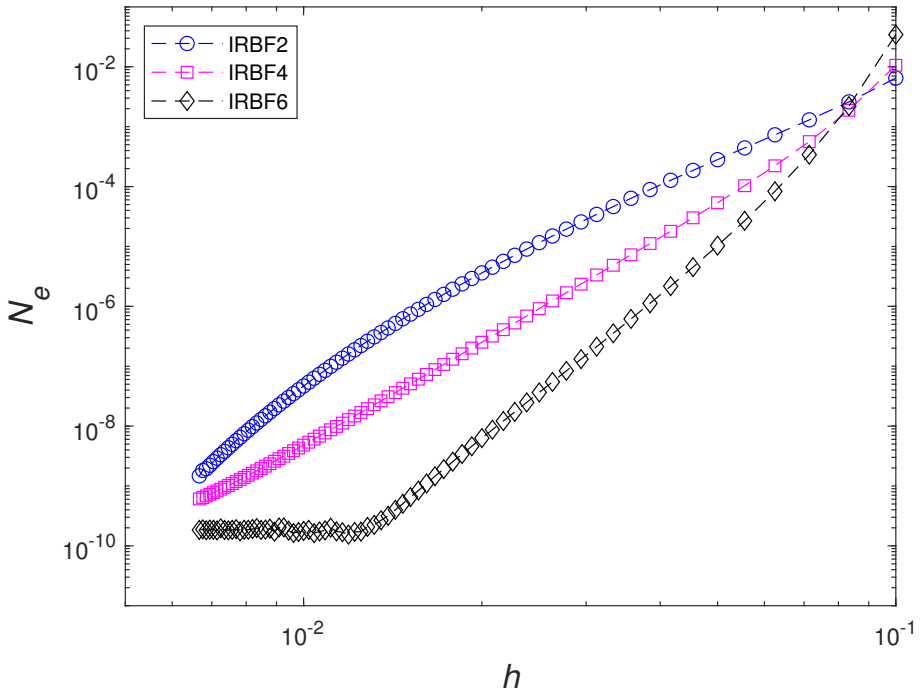

Figure 14: Poisson equation, mixed precision, $N_x = N_y = (11, 21, \cdots, 151)$, variable width: Plots of the solution accuracy versus grid size for IRBF2, IRBF4 and IRBF6 employed with their largest widths. The higher the order of the IRBF scheme the more accurate the solution will be: $O(h^{5.74})$ for IRBF2, $O(h^{5.84})$ for IRBF4 and $O(h^{9.38})$ for IRBF6. It is noted that a tolerance of 10^{-10} is used in the Picard-type iteration scheme.

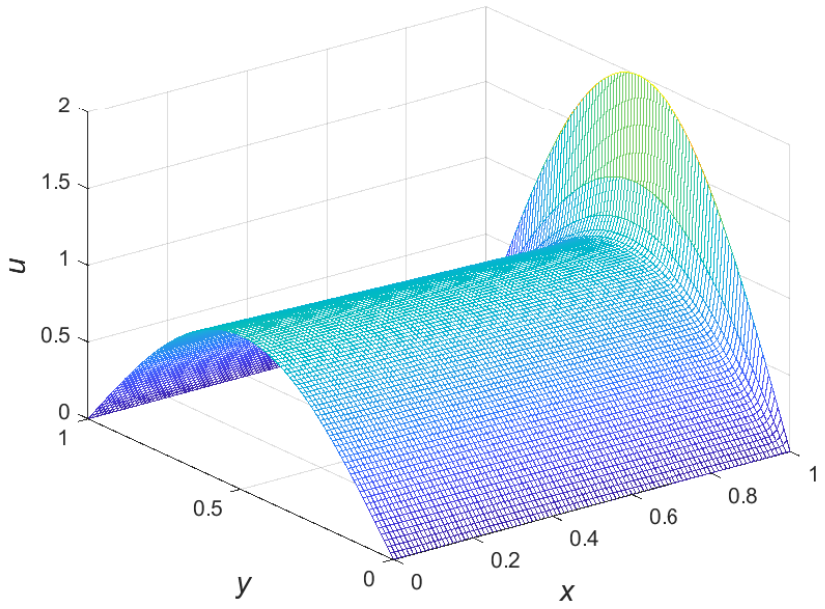

Figure 15: Convection-diffusion equation, $\varepsilon = 0.01$: Exact solution.

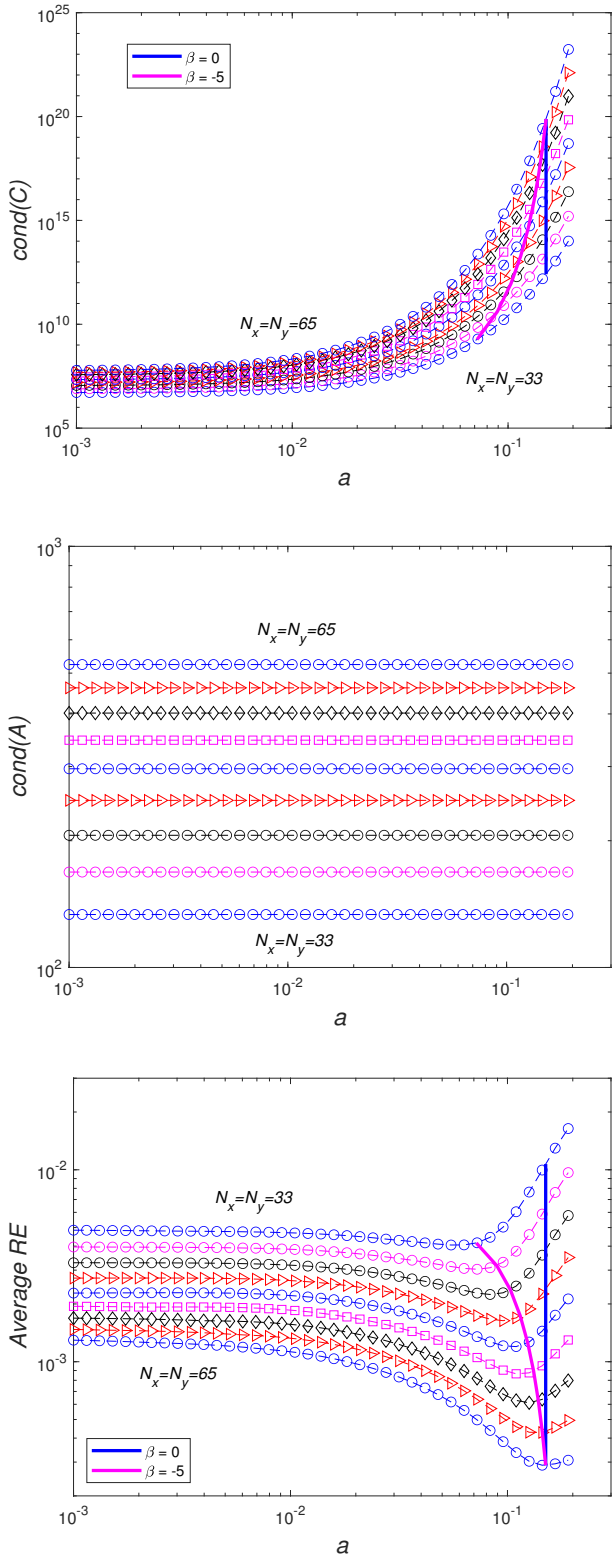

Figure 16: Convection-diffusion equation, $\varepsilon = 0.01$, mixed precision, IRBF2, $N_x = N_y = (33, 37, \cdots, 65)$: Plots of the matrix condition numbers and the solution accuracy versus the RBF width for several grid sizes. For a given grid size, the RBF width has a strong effect on the condition number of the conversion matrix and no effect on the condition number of the system matrix. The condition number is high for the conversion matrix and low for the system matrix. Results by two different ways of implementing the RBF width, fixed ($\bar{a} = 0.15,\ \beta = 0$) and variable ($\bar{a} = 0.15,\ \beta = -5$) values with grid refinement, are also included. The variable-width case generally yields more accurate results than the fixed-width case.

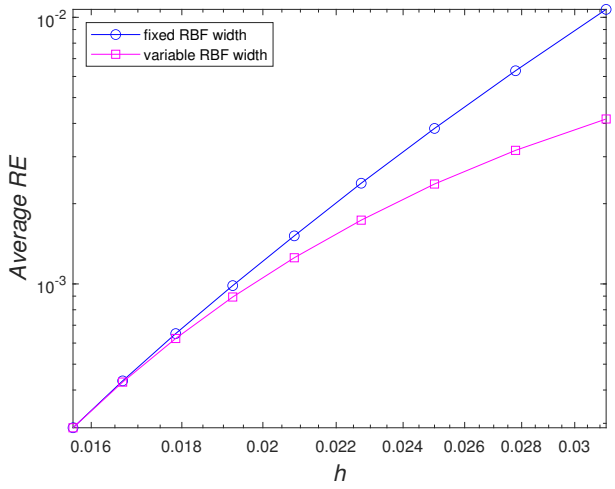

Figure 17: Convection-diffusion equation, $\varepsilon = 0.01$, mixed precision, IRBF2, $N_x = N_y = (33, 37, \cdots, 65)$, $\bar{a} = 0.15$: Plots of the solution accuracy versus grid size for the fixed ($\beta = 0$) and variable ($\beta = -5$) width cases. The errors reduce quick for both cases, $O(h^{5.20})$ for the fixed width and $O(h^{3.82})$ for the variable width. The latter yields higher levels of accuracy but a slower average rate of convergence than the former.

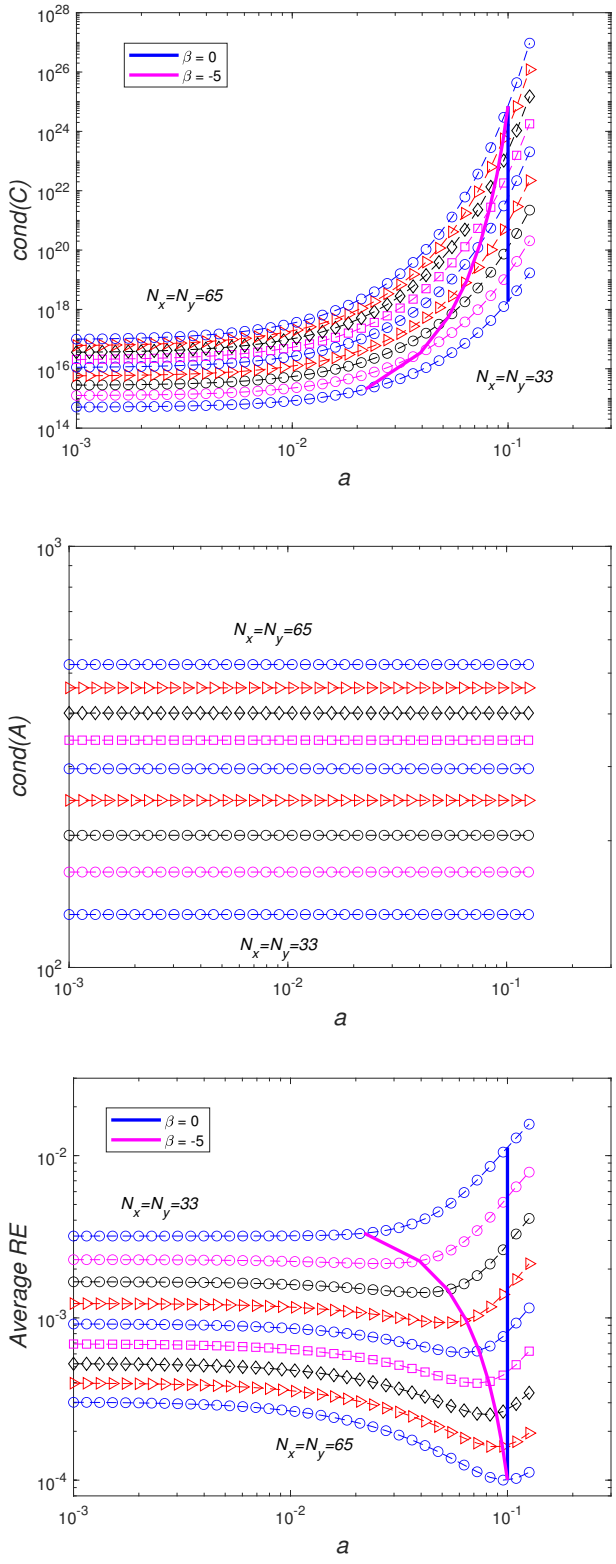

Figure 18: Convection-diffusion equation, $\varepsilon = 0.01$, mixed precision, IRBF6, $N_x = N_y = (33, 37, \cdots, 65)$: Plots of the matrix condition numbers and the solution accuracy versus the RBF width for several grid sizes. For a given grid size, the RBF width has a strong effect on the condition number of the conversion matrix and no effect on the condition number of the system matrix. The condition number is high for the conversion matrix and low for the system matrix. Results by two different ways of implementing the RBF width, fixed ($\bar{a} = 0.1,\ \beta = 0$) and variable ($\bar{a} = 0.1,\ \beta = -5$) values with grid refinement, are also included. The variable-width case generally yields more accurate results than the fixed-width case.

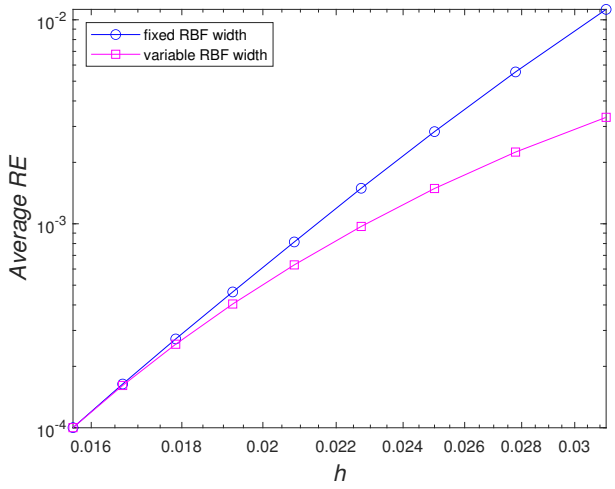

Figure 19: Convection-diffusion equation, $\varepsilon = 0.01$, mixed precision, IRBF6, $N_x = N_y = (33, 37, \cdots, 65)$, $\bar{a} = 0.1$: Plots of the solution accuracy versus grid size for the fixed ($\beta = 0$) and variable ($\beta = -5$) width cases. The errors reduce quick for both cases, $O(h^{6.83})$ for the fixed width and $O(h^{5.05})$ for the variable width. The latter yields higher levels of accuracy but a slower average rate of convergence than the former.

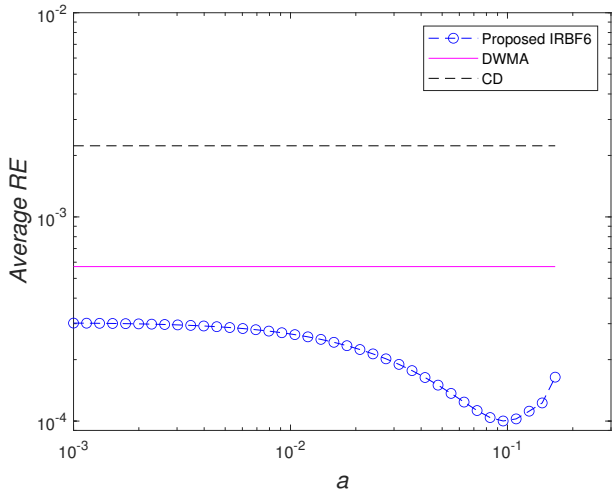

Figure 20: Convection-diffusion equation, $\varepsilon = 0.01$, mixed precision, IRBF6, $N_x = N_y = 65$: Comparison of the solution accuracy between the central difference (CD), discrete weighted mean approximation (DWMA) and IRBF6 schemes. These schemes are all based on local stencils of 5 points. For a wide range of the RBF width employed, results by the proposed scheme are more accurate than the other two results that are extracted from [28].